ADVANCED NANOMECHANICAL TESTING

A novel nanoindentation protocol to characterize surface free energy of superhydrophobic nanopatterned materials

E. M. Rossi[1], P. Sudharshan Phani[2], R. Guillemet[3], Julie Cholet[3], Doriane Jussey[3], W. C. Oliver[4], M. Sebastiani[1,a])

[1] Engineering Department, Università Degli Studi Roma Tre, via della Vasca Navale 79, 00146 Rome, Italy
[2] International Advanced Research Centre for Powder Metallurgy & New Materials (ARCI), Hyderabad, Telangana 500005, India
[3] Thales Research & Technology, Avenue Augustin Fresnel, 91767 Palaiseau Cedex, France
[4] KLA Corporation, 105 Meco Ln, Oak Ridge, TN 37830, USA
a) Address all correspondence to this author. e-mail: marco.sebastiani@uniroma3.it

Surface Free Energy (SFE) has become a relevant design parameter to produce materials and devices with controlled wettability. The non-destructive measurement of SFE in nanopatterned super-hydrophobic hard surfaces is a challenge in both research and industry since in most cases time-consuming contact angle measurements are not feasible. In this work, we present a novel nanoindentation based method for the measurement of pull-off adhesive forces by carefully controlling environmental and instrumentation issues. The method is found to measure SFE over five orders of magnitude, covering hydrophilic to super-hydrophobic surfaces, and has been validated with contact angle measurements. Its limitations and shortcomings are critically discussed, with a specific focus on the experimental issues that could affect the reliability and reproducibility of the results. Finally, the potential applications of the newly developed methodology include fast non-destructive mapping of SFE over heterogeneous surfaces with spatially controlled wettability.

Introduction

The ability to engineer and control surface free energy and wettability of functional materials is critical in industry, e.g. microelectronics, microsystem engineering, energy, photonics, tribology, tissue engineering and biomedical devices [1–9]. Contact mechanics related problems, such as the uncontrolled adhesion of surfaces with complex shape and geometries, hugely affects the products and their applications in these sectors [10–14]. These problems arise from intertwined physicochemical properties of the contacting surfaces and the interfaces between them. The characterization of these surface and interface properties is important for reliability, reproducibility, and the ability to design a system with predictable performance. Specifically, in recent years, micro-actuators, engineered scaffolds for tissue regeneration, nano-patterned super-hydrophobic or hierarchically structured surfaces, micro/nanoparticles for drug delivery, and coatings for biosensors are examples of industrial applications where the problem of nano-scale adhesion must be addressed through an accessible, meaningful and high-throughput way [15–19].

Furthermore, the complex mechanisms determining wettability, adhesion and friction on nanopatterned materials also require the use of multiple techniques that can provide a quantitative characterization at multiple length scales, in both lateral dimensions and depth, underpinned by sound physical models that are validated experimentally [20, 21]. Indeed, the assessment of wettability, adhesion, and friction at the micro- and nanoscales has become an extremely important scientific and industrial problem that is unresolved. In some cases, conventional methods like contact angle measurement (CAM) are not feasible because of the limited amount of available surface area and/or the use of non-planar substrates. As a result, many of the

FOCUS ISSUE

high-value products suffer from poor yield, low productivity, and unreliable end-use performance.

For instance, by using Young's equation and different models (e.g. Owens–Wendt, Fowkes, Good–Girifalco, van Oss–Chaudhury–Good [22]), the total surface free energy and its dispersion and polar components can be determined by CAM [23]. However, the application of such models requires the use of multiple liquids over a relatively large area for testing, to perform the experiments in compliance with current international standards. Besides, the use of some of the liquids (e.g., methylene iodide) can lead to damage and/or degradation of the surface. Therefore, the development of novel non-destructive methods is a strong scientific and technological need, to achieve a fast, reliable, and non-destructive assessment of surface energy on small areas of nano-patterned surfaces.

Nanoindentation testing [24, 25] can offer a possible contact-mechanics methodology that allows measurement of intrinsic surface properties like surface free energy of materials [26, 27]. Through this technique, it is possible to measure the force required to separate the indenter tip from the sample surface [24, 28]. This force is usually called either the "pull-off force" or the "adhesion force" and it can be experimentally obtained from the load–displacement curve. The latter is then used to estimate the work of adhesion, which, in the case of identical contacting surfaces, is twice their surface free energy (see Fig. 1, where also the "snap-in" or "jump-to-contact" event is depicted).

Different continuum contact mechanics models have been developed to obtain the work of adhesion and surface free energy from the experimentally determined pull-off force. Of these, the two major ones are the Derjaguin–Muller–Toporov (DMT) model, which accounts for the long-range surface forces outside the contact area, and Johnson–Kendall–Roberts (JKR) model, evaluating the work of adhesion from the force required to separate two elastic bodies having a certain radius of curvature. The details of the contact mechanics of these models are discussed elsewhere [29–35]. A series of experimental reports have already assessed the validity of both JKR and DMT approaches [36–39], showing that the two models represent the boundaries of the adhesion mechanisms domain. In particular, the JKR model is accurate for describing the contact between compliant bodies, where large elastic deformations prevail. On the contrary, the DMT model better describes the interaction between stiff bodies where the contact radius is small. In both cases, the models consider the surface adhesive forces as an additional contribution to the normal load (in comparison with the classical Hertz theory, where surface forces are not considered at all). In a later paper, Maugis has described comprehensively the possibility of having intermediate cases between JKR and DMT regimes, by proposing a transition parameter λ describing different adhesive contact regimes [38]. The main assumptions of the models, together with the basic equations adopted for SFE calculation, are described in Fig. 1. In both cases, the SFE of the sample (γ_2) can be evaluated from the measured pull-off force, by knowing the tip radius (R) and surface energy of the indenter (γ_1). Clearly, both models assume the sample to be an infinite half-space.
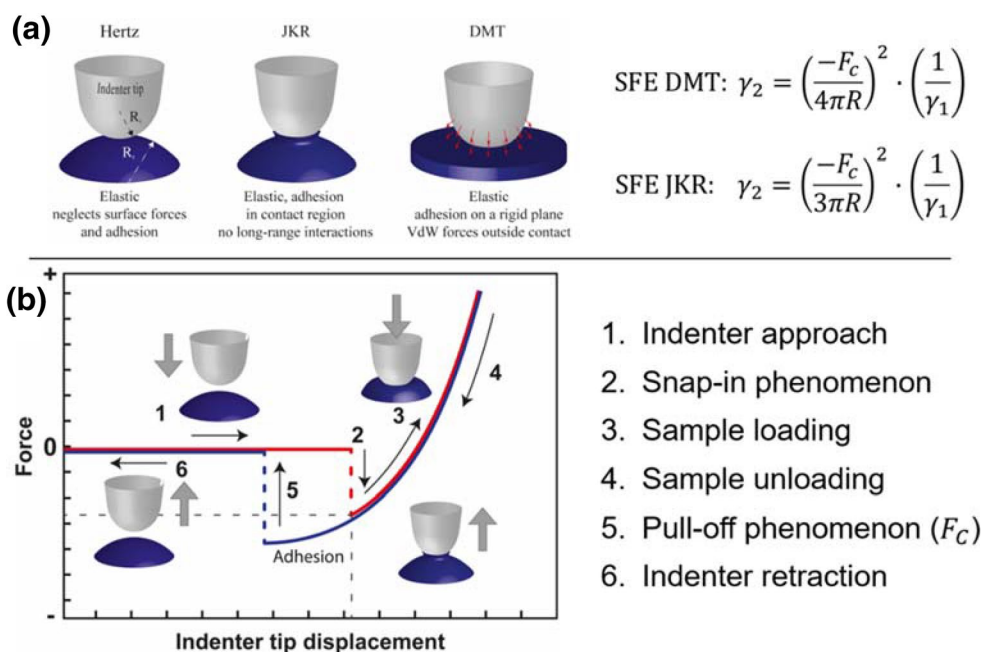

Figure 1: (a) Contact mechanics models for the assessment of the free surface energy at the micro- and nanoscale. (b) Theoretical nanoindentation Force–Displacement curve accounting for free surface energy related phenomena (snap-in and pull-off).

$$\text{SFE DMT: } \gamma_2 = \left(\frac{-F_c}{4\pi R}\right)^2 \cdot \left(\frac{1}{\gamma_1}\right)$$

$$\text{SFE JKR: } \gamma_2 = \left(\frac{-F_c}{3\pi R}\right)^2 \cdot \left(\frac{1}{\gamma_1}\right)$$

1. Indenter approach
2. Snap-in phenomenon
3. Sample loading
4. Sample unloading
5. Pull-off phenomenon (F_C)
6. Indenter retraction

Irrespective of the applicability or accuracy of the adopted contact models, which are not detailed and discussed in this article, the experimental determination of pull-off forces in case of hard nanopatterned surfaces is very challenging, as (i) a purely elastic contact should be maintained to avoid damage to the surface structures and (ii) the resulting pull-off forces are usually of the same order of magnitude of the commercial nanoindentation systems noise floor values.

A recent study has proposed the use of a specifically designed MEMS-based actuator (with a lower moving mass in comparison with standard nanoindentation systems) to improve sensitivity and resolution for the assessment of adhesive forces by nanomechanical experiments [40]. However, the objective of the present work is the development and validation of a novel testing protocol that uses commercially available actuators with minor hardware modifications, achieving wider feasibility of the nanoindentation SFE measurements.

On this basis, the developed experimental procedure allows the determination of the surface free energy of stiff/hard nano-patterned surfaces, without altering the original morphology, by using the nanoindentation equipment in a non-conventional mode. The new protocol includes modifications of the force actuator to improve sensitivity and resolution, as well as a novel testing procedure to minimize spring-stiffness, damping and acceleration effects. The developed method has been thoroughly validated on different hydrophilic and hydrophobic reference surfaces, and then applied to nanopatterned super-hydrophobic materials to demonstrate that it can measure surface energy values over five orders of magnitude.

Results

Fabrication of nanopatterned samples and contact angle measurements

A set of reference surfaces was selected to test and validate the nanoindentation hardware modifications and the novel developed method: (i) muscovite mica provided highly energetic, new, and atomically flat surfaces via cleavage of its sheet-based silicate structure; (ii) germanium (100) crystals yielded the reference substates for the development of super-hydrophobic surfaces.

The reduction of the surface free energy of the reference germanium surfaces was tackled by both patterning and functionalization. The effects of those processes were independently studied on flat fluorinated silane coated substrates (silanized) and nano-patterned surfaces. The interplayed role of both patterning and functionalization was then investigated on nanopatterned and silanized germanium substrates. A detailed description on processing of the studied samples, for which a schematic is reported in Fig. 9a, is presented in the Methodology section of the present work.

Contact angle measurements were performed on all the surfaces investigated to provide comparative results for the validation of the novel nanoindentation method. Those outcomes are shown in Table 1. CAMs reveal a clear transition from a hydrophilic behavior for the flat reference samples (mica and germanium) to hydrophobic for the silanized sample, and to super-hydrophobic for the nano-patterned and silanized sample (see Fig. 2). In the case of the two reference flat samples (mica and germanium), we found reasonable agreement between contact mechanics results (with both adopted sphero-conical tips) and the contact angle measurements. On the contrary, the two methods seem to give different results for the case of surface-treated and nano-patterned samples. Still, the trend remains identical in both cases, showing a transition from hydrophilic to super-hydrophobic for the case of the patterned and silanized germanium sample. CAM with the three liquids was not possible in all cases: for the mica sample, the measurement with formamide was not feasible because of the spontaneous spreading behavior of the droplets, resulting in unstable contact angle values. In case of the patterned and silanized germanium, water contact angle was not possible because of the extreme hydrophobic behavior Fig. 2e). A video of this latter phenomenon is given in the supplementary material. The minimum available testing area of the patterned germanium sample (only a small piece of the patterned sample was taken before the silanization process), limited the measurements only to water contact angle.

TABLE 1: Summary of contact angle measurements and Owens–Wendt calculated SFE values on all the samples analyzed.

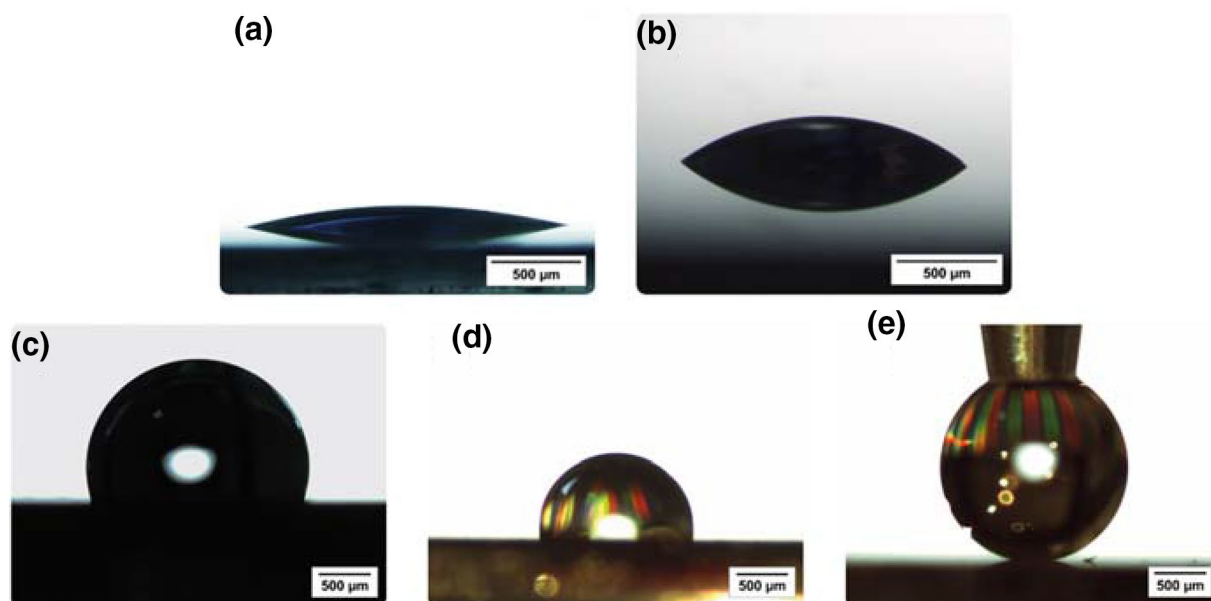| Sample	Water (deg)	Diiodomethane (deg)	Formamide (deg)	SFE Owens Wendt (mJ/m^2)
Mica	19 ± 3	49 ± 2	n.a	70 ± 2
Bare germanium	51 ± 2	42 ± 4	40 ± 4	53 ± 3
Silanized germanium	103.9 ± 1.3	96 ± 1.67	95 ± 1.5	13 ± 1
Patterned germanium	88 ± 3	n.a	n.a	n.a
Patterned and silanized germanium	n.a	106 ± 4	116 ± 2	4.45 ± 0.71

Figure 2: Representative water contact angle measurements for (a) flat mica crystal, (b) flat germanium wafer, (c) silanized flat germanium, (d) nano-patterned germanium and (e) nano-patterned and silanized germanium.

Optimized nanoindentation method and testing protocol

Determining the SFE from pull-off force during an instrumented indentation test is a simple and hence attractive option, especially for small volumes of material, wherein conventional techniques may not be feasible [41]. However, given the typical order of magnitude of the pull-off forces (µN) for hard/stiff materials, extreme caution needs to be exercised during the measurements with a commercially available nanoindentation system (typically designed to operate in the mN range). Of the several factors that can potentially influence the measurements, the instrument's dynamics and electronic contribution, thermal stability, testing environment and test protocol play a major role in making reliable measurements. In this work, a commercially available Nanoindenter, iNano® Nanoindenter (Nanomechanics Inc., KLA corporation, Oak Ridge, USA) has been specifically modified to enable accurate measurement of the pull-off forces. As a logical next step to the hardware modifications, a novel test protocol is also developed to leverage the new hardware capabilities.

As mentioned earlier, the key to reliable adhesion measurements is the ability to accurately measure forces in the µN range along with low noise levels. The latter are achieved using a new high-resolution electromagnetic force actuator, designed to exert a maximum force of 5 mN (instead of the conventional limit of 50 mN of the InForce50 actuator from KLA-Nanomechanics), which enables an improved Signal-to-noise ratio (SNR). This new high SNR force actuator, considering the inherent linearity of the electromagnetic actuated, leaf-springs supported assembly, enables the instrument to be accurately modelled as a single degree of freedom oscillator with a mass of 259.8 mg, damping coefficient of 0.106 Ns/m and spring stiffness of 716 N/m, and thereby provides a simple way to account for the instrument's dynamic contribution to the load for enhanced load accuracy, as detailed elsewhere [42].

To leverage the enhanced hardware capabilities, the test protocol is also modified to further improve the accuracy and precision of the measurements. While the hardware modifications enable accurate force measurements by accounting for the instrument's contribution, it is imperative to perform the tests under conditions in which this contribution is anyway minimal. A typical mechanical system has force contributions from the spring, damper, and mass. The spring constant of the actuator is specifically designed to be higher than the typical value of ~ 100 N/m to minimize the instability due to the strong adhesive forces on highly hydrophilic materials, which could cause uncontrolled early loss of contact and, therefore, a significant underestimation of the pull-off force and inaccurate measurement of the surface free energy. This phenomenon is particularly pronounced in AFM experiments, where a low cantilever stiffness usually gives unstable jump-to-contact and pull-off events. The use of a higher spring stiffness in this work minimizes this issue. In situations where the indenter rings after loss of contact, using the high data acquisition rate and short displacement time constant signal, it has been ensured that the indenter does not contact the sample surface again after pull-off.

The other mechanical contributors are damping and inertia, which depend on velocity and acceleration, respectively.

Figure 3: Typical Load vs. Displacement Into Surface response using a standard test protocol, highlighting several experimental issues.
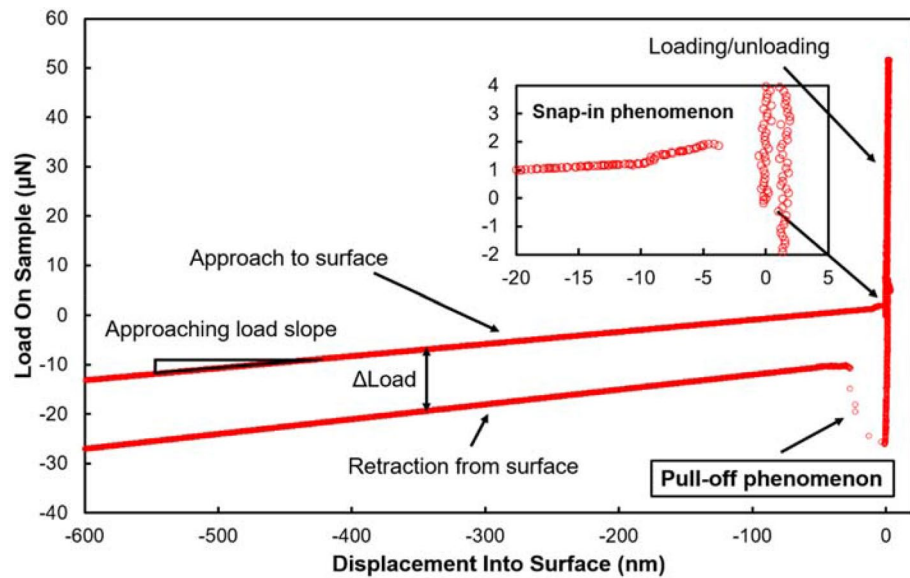
These contributions can be minimized by low approach velocities (< 5 nm/s). However, low approach velocities result in longer testing times, a large fraction of which is not in contact with the sample, possibly contributing to the thermal drift. Some of the typical issues encountered in measuring an accurate load–displacement response at low loads using the standard test protocols are illustrated in Fig. 3, in the case of a germanium (100) wafer with an approach velocity of 100 nm/s starting from 1000 nm above the surface. It may be noted that

the maximum load is limited to 50 µN to highlight the issues at low loads. The approach and retraction segments have a slight slope and are also separated by a delta in the force values of ~ 20 µN. While this is a small deviation for a typical indentation test (where the loads are in mN range), it is a significant fraction of the pull-off force for an adhesion experiment.

The schematic representation of the new test protocol is shown in Fig. 4, along with a typical displacement–time and load–displacement response. The modified procedure involves
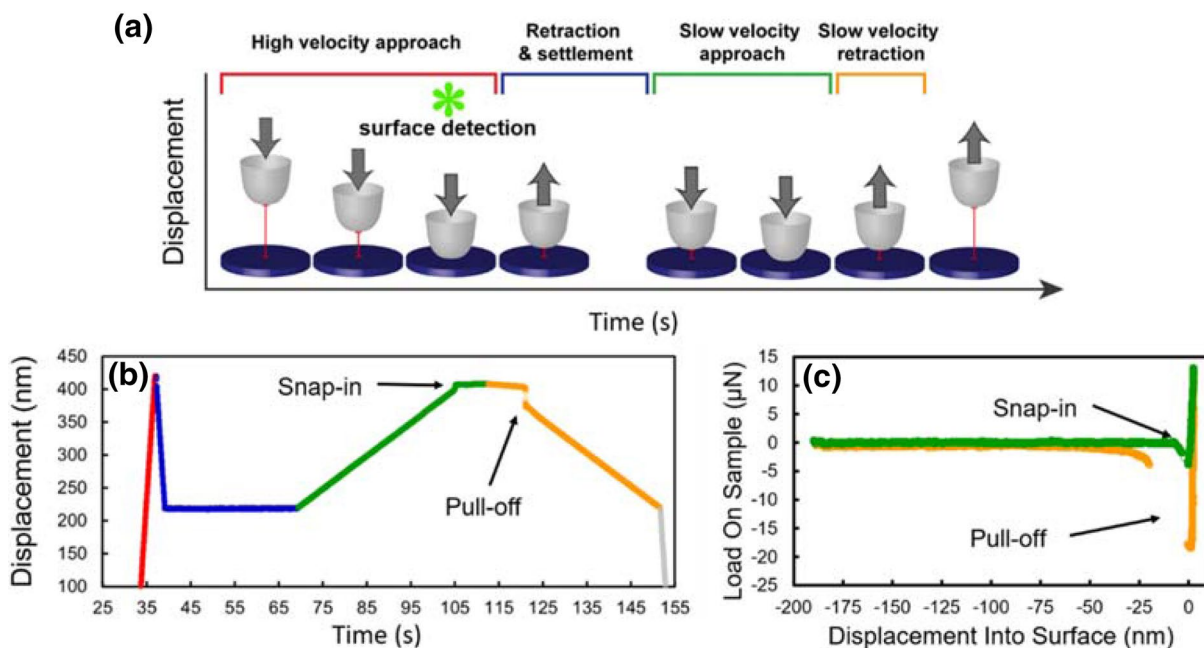

Figure 4: (a) Schematic of the new test protocol. (b) displacement vs time curve during the different highlighted segments of the procedure and (c) the corresponding Load vs. Displacement curve.

a two-step surface approach, wherein the surface is initially detected at a fast approach velocity of 100 nm/s. Subsequently, the indenter is retracted to a position very close to the surface (100 nm) and allowed to stabilize before starting a second approach at a very low velocity of 2–5 nm/s. This procedure has several advantages compared to the standard technique shown in Fig. 3, such as (i) a significant reduction in the overall time required to perform a test, owing to the initial fast approach and the extremely limited distance from the sample surface at which the second slow-velocity one is performed, while, due to the latter, (ii) still greatly reducing the instrument's damping and inertial contributions. Also, allowing the system to stabilize at a position very close to the surface minimizes any thermal gradient that could contribute to the displacement drift. A low approach velocity (5 nm/s) provides an accurate estimate of the spring constant at the location of the test. The algorithm used for surface detection also plays a key role in this method, not only for an accurate calculation of load, but also to ensure elastic contact during the first approach. Using a high data acquisition rate (1 kHz) coupled with a low-noise (~ 0.25 nm) displacement sensor of 20 μs time constant, the surface position and the loading can be accurately determined and controlled, based on small deviations from threshold value of the tip velocity. Figure 4c shows the load–displacement response measured with the new

test protocol with the maximum load limited to around 10 μN. The issues with the accuracy of spring and damping correction, typically encountered in the standard test protocol (see Fig. 3) have been successfully overcome, with a flat and overlapped load–displacement response during loading and retraction. The typical RMS value of the load during approach is less than 0.5 μN (with values reaching below 0.21 μN when testing at the smallest viable velocities for the lowest SFE samples), which is still an order of magnitude lower than the pull-off force for samples exhibiting low surface free energy values, thereby enabling accurate adhesion measurements. It may also be noted that the load–displacement data for the loading and unloading segments are almost identical, thereby demonstrating a purely elastic response and the efficacy of the surface detection and loading criteria at both the high and low velocity approaches.

For the present investigation, two different sphero-conical tips were used, with a radius of 52.5 μm and 15.8 μm. In this way, a comprehensive validation on the reference materials and sensitivity analysis was possible as will be presented in subsequent sections.

Results of Surface Free Energy (SFE) measurements

Figure 5 reports the representative load–displacement curves for the mica and germanium flat reference samples using the
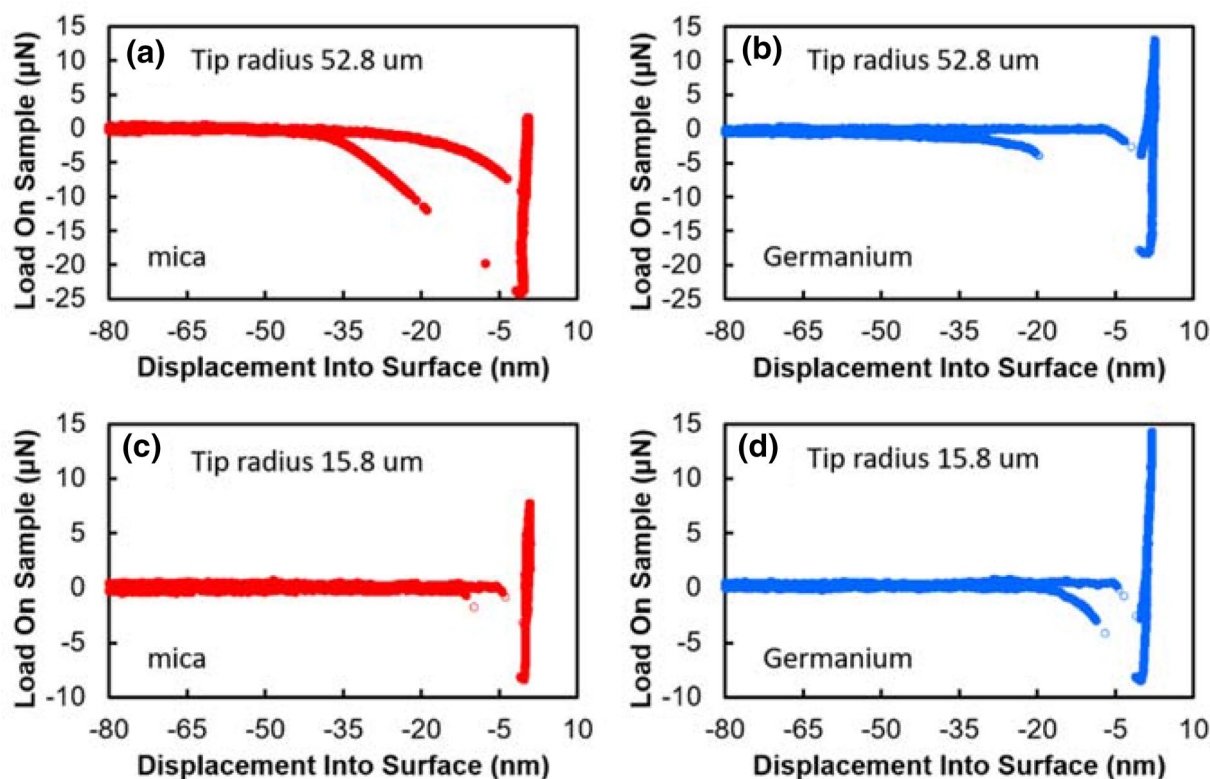

Figure 5: Representative Load – Displacement Into Surface curves on flat mica and bulk germanium samples with no-surface functionalization, using a 52.8 μm sphero-conical indenter tip (a–b) and a 15.81 μm sphero-conical tip (c–d).

two different tips. As discussed in the previous section, with the new test protocol, the load–displacement data during the approach and retraction segments are flat and characterized by minimal noise levels (i.e. of an order of magnitude lower than the pull-off forces). The maximum load has been appropriately controlled to ensure purely elastic contact, as evidenced by the reversibility of the load–displacement data during loading and unloading, thereby enabling the accurate determination of snap-in and pull-off phenomena according to the selected SFE-accounting contact mechanics models. The data clearly show a reduction in the pull-off force with decreasing tip radius, as predicted by models.

Figure 6 shows the surface free energy (SFE) obtained by nanoindentation (both JKR and DMT models), in comparison with the conventional contact angle method. Very good agreement between the nanoindentation based method and contact angle method can be observed, with the latter yielding results between the two extreme cases (JKR and DMT) of adhesion models used in nanoindentation method. It is also worth noting that values obtained by nanoindentation with the two different tips are also in good agreement, thus validating the new testing protocol. A larger tip radius results in higher pull-off forces, thereby improving the sensitivity of the measurements, which is especially beneficial for hydrophobic materials. Henceforth, results from the larger, **52.8 μm** sphero-conical tip will be presented.

The results of nanoindentation based adhesion measurements on mechanically and chemically functionalized germanium samples, which exhibit hydrophobic and superhydrophobic response, are shown in Fig. 7. In this case, we observe a significant reduction of the pull-off force compared to the flat untreated samples. For the flat silanized sample, the measured pull-off force is still significantly higher than for the case of the two nano-patterned materials, while the lowest pull-off force is measured for the nano-patterned and silanized germanium.

In the latter case (super-hydrophobic behavior), it is crucial to ensure that the surface approach and retract load-depth curves are perfectly flat (precise spring calibration) and without any separation (correct damping calibration). Any deviations thereof should be addressed by appropriate calibration to minimize the experimental artifacts.

Finally, a summary of all nanoindentation based SFE measurements, using both the JKR and DMT models (Fig. 1), is shown in Fig. 7d (exact values are provided in the supplementary Table I to the present work). As previously discussed, these two models represent the possible extremes for adhesive contact regimes encountered during the experiments. Note that the surface free energy is plotted based on a logarithmic scale which highlights the ability of the present method to measure SFE over several orders of magnitude using a single instrument and test protocol.

Discussion

Novel test protocol for adhesion measurement

The main purpose of the present work was to develop and validate a non-destructive method for fast and reliable measurement of surface free energy (SFE) on hard super-hydrophobic nanopatterned surfaces. To this end, an optimized nanoindentation protocol was developed, allowing for reliable measurement of contact forces in the μN range. The key factor for enabling force measurements in this range is the fine control of the various factors affecting force measurement, which, as mentioned previously, include precise control of the testing environment, spring stiffness, thermal drifts, damping and acceleration effects. The proposed method allows to achieve this in two different, but complementary ways: (a) careful design of the force actuator to enable application of limited forces coupled with accurate calibration of the system under controlled atmosphere; and (b) robust dynamic modelling of the system to account for the instrument's spring, damper, and mass contributions.
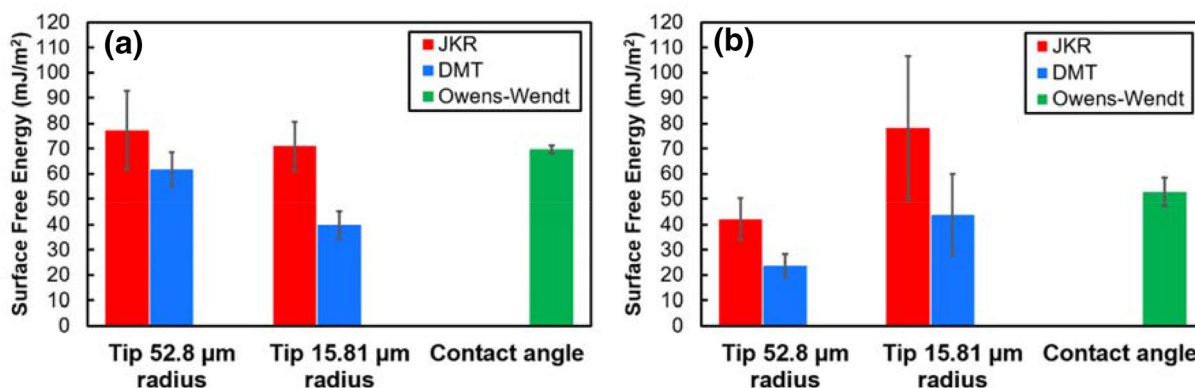

Figure 6: Comparison of surface free energy obtained from different techniques on (a) mica and (b) bulk germanium with no-surface functionalization.
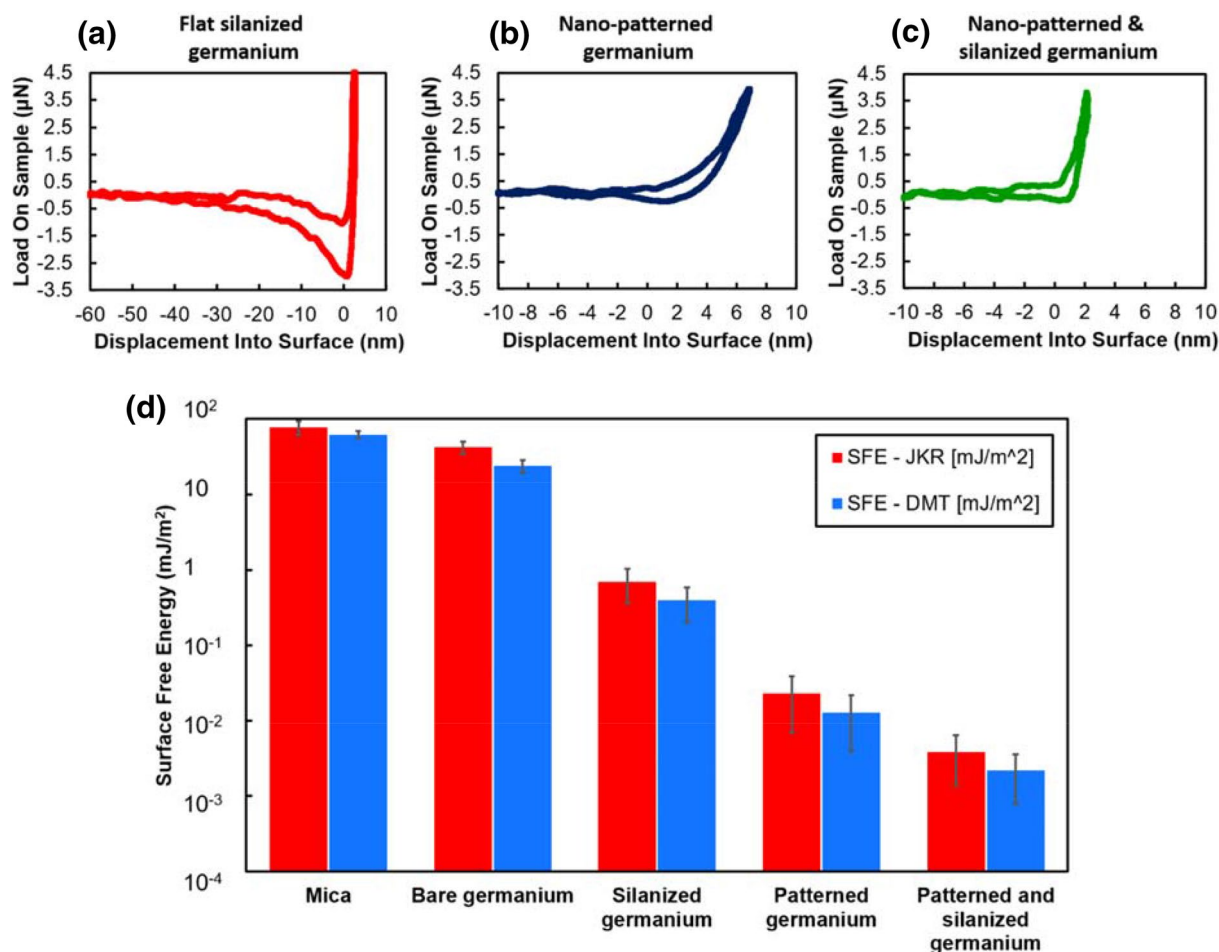
Figure 7: Representative load-displacement curves for measurements with a 52.8 μm sphero-conical tip, on mechanically and chemically functionalized germanium samples. (a) flat silanized germanium, (b) nano-patterned germanium and (c) nano-patterned and silanized germanium. (d) Comparison of surface free energy measured on mechanically and chemically functionalized germanium substrates – data are represented on a logarithmic scale.

The newly developed method minimizes the instrument's contribution to the overall measurement and the experimental issues arising from thermomechanical effects and damping effects, by using an improved actuator (higher spring stiffness, improved force resolution) and a two-step surface approach procedure. In this way, the RMS noise on force measurement can be controlled to reach and stay below values of around 0.21 μN, and a purely elastic contact is achieved also in case of the nano-patterned samples, with a maximum contact force of about 5 μN while still retaining a high throughput. The developed protocol has been validated on two reference flat materials with independently measured SFE values, obtained by contact angle measurements, and using two sphero-conical diamond tips with different radius of curvature. The proportional reduction of the pull-off forces with decreasing indenter tip radius and the agreement in the SFE is a strong evidence that the surface contact forces are correctly being measured.

By using this validated protocol, the method was demonstrated to be able to measure surface energy on hydrophobic and super-hydrophobic materials, over a SFE range of five order of magnitude. In addition, the method allows performing a large number of experiments over wide areas, since a single measurement takes less than 2 min and is completely non-destructive. This aspect is particularly relevant for the nanopatterned surfaces under investigation, where one of the main industrial challenges is to perform mapping of adhesive properties over non-planar substrates, with the aim of developing surfaces with spatially tailored surface energy and wettability.

While the method presented here bears several advantages, it is instructive to also highlight its limitations and key experimental aspects for reliable measurements. First, a fine control of all experimental parameters and testing environment is extremely important. Tip and sample cleaning and humidity control are critical. Another important aspect of the method

is the ability to determine the spring stiffness, damping coefficient and mass of the actuator, which can significantly affect the measured pull-off forces. Additionally, in case of extremely hydrophilic materials, which are not under investigation in this work, an instability due to the support springs can occur during pull-off. In this case, it is preferable to use a tip with smaller radius to reduce the magnitude of the pull-off force. If the above-mentioned aspects are carefully addressed, we believe that it is possible to perform reliable and reproducible adhesion measurements via nanoindentation.

Comparison of the different adhesion measurement techniques

The comparison with contact angle measurements (CAM) is a critical factor for validation and possibly industrial exploitation of the method developed in this work. As reported in Table 1, a very good agreement exists between CAM and nanoindentation results on the flat reference samples. However, the two methods yield significantly different results in case of the super-hydrophobic materials, even if a very low SFE value is calculated in both cases. There are two possible explanations for the observed discrepancy. First, there is a transition from Wenzel to Cassie-Baxter wetting regimes [20, 43, 44] in case of the contact angle measurements of super-hydrophobic materials (Fig. 8a–b). Since Wenzel and Cassie-Baxter regimes refer strictly to wettability, there is no direct correlation with a nanoindentation experiment of a nanopatterned surface.

In fact, in case of the nanoindentation tests the actual area of interaction between the tip and the sample is significantly reduced for the nano-patterned surface, an effect that is not

considered by the JKR and DMT models used to calculate the SFE values. A schematic representation of this configuration is shown in Fig. 8c, where the actual geometry of the samples under investigation differs significantly from the half-space assumption that is inherent in JKR and DMT models. If the contact area and effective contact radius are corrected to account for the actual surface geometry of the sample, which consists of high aspect ratio cones with tip curvature of about 50 nm, a better agreement is expected. In this way, the evaluated SFE value for a given pull-off force value would be higher than the one corresponding to the half-space situation.

An approximate calculation of the actual contact area could be performed by assuming that the cones are truncated with a top-area of 50×50 nm^2. Under this assumption, an average number of four cones are in contact with the indenter when the displacement into surface is of 5 nm, corresponding to a contact area of the order of 10^4 nm^2. This value is two orders of magnitude lower than the one obtained (for the same displacement into surface of 5 nm) by using the classical Hertz theory of elastic contact. While this simple estimation provides a general idea of the extent of area reduction, the fully elastic deformation regime achieved during testing, combined with an extremely limited ratio between the pattern periods investigated (2.4 μm) and the characteristic lengths of the indenter tip (selected 52.8 μm radius), ensures the complete applicability of the adopted models.

Finally, it worth discussing the comparison between the present method and other available techniques in the literature. A large body of literature exists on adhesion measurements on soft materials, biological tissues, and atomically flat surfaces by atomic force microscopy (AFM) [39, 47, 48]. While the force range of interest in the present work is well within AFM regime, the inherent nature of the AFM technique which is optimized for greater flexibility to enable high contrast topography measurement, naturally compromises the ability to accurately measure force. As AFM's are designed to be multiple degrees of freedom oscillators, accurately factoring out the instrument's dynamic contribution to the force is challenging, unlike the nanoindentation system which is designed to be a single degree of freedom oscillator [49]. Additionally, the use of AFM for mechanical characterization of nanopatterned hard materials can lead to fast degradation of the tips.

Another possibility is the use of a Surface Force Apparatus (SFA), which is specifically designed for surface energy measurement based on the surface contact forces between two identical materials as detailed by Israelachvili et. al. [50, 51]. In case of SFA, the displacement is measured by means of an optical method, and the geometry and nature of the samples is thus strongly limited. In fact, the use of the optimized nanoindentation protocol presented here allows for the measurement of SFE
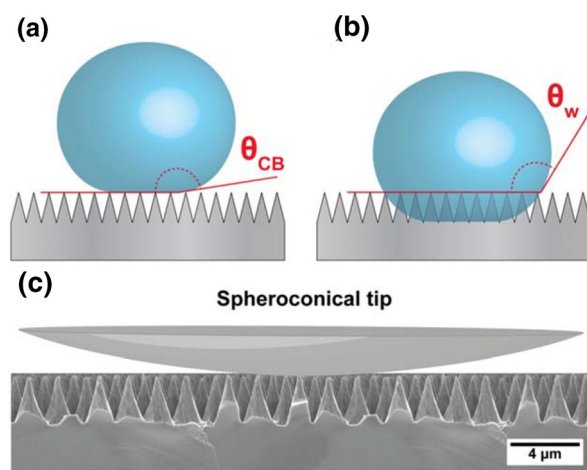

Figure 8: (a) Cassie-Baxter wetting regime and (b) Wenzel wetting regimes compared to the contacting regime of a sphero-conical indenter tip schematized in (c) overlaid to the FIB cross-section (micrograph of the actual sample) of a nano-patterned hydrophobic Germanium sample.

on complex nano-architected materials, which is quite challenging by conventional methods.

In summary, the use of an improved nanoindentation method seems to be an optimal solution for those applications where fast mapping of surface free energy is required for design and optimization on new materials with tailored wettability. A non-destructive technique is very useful in those cases where water contact angle measurement is not possible because of an extreme hydrophobicity.

Applications where this method can be extremely useful comprise avionics and optics, where there is a strong need for the development of non-planar transparent surfaces with hydrophobic (still mechanically robust) behavior. Potential future developments of the method could be the use of high-speed nanoindentation for fast mapping [52] of adhesion forces over large areas, as well as the use of this tool for in-line non-destructive measurement of surface energy.

Conclusions

In this paper, an improved and optimized nanoindentation protocol is presented for surface free energy (SFE) measurement on hard nano-patterned super-hydrophobic materials. By carefully controlling environmental and instrumentation aspects, adhesion forces lower than 0.5 µN can be measured.

The validation on selected reference materials showed very good agreement with SFE values obtained by contact angle measurements, while the application on hydrophobic and super-hydrophobic materials has shown that this method can measure SFE values over a range of five orders of magnitude. Besides, the method can be particularly useful in situations where contact angle measurement is not possible (either due to limited available testing area, or extreme hydrophobic behavior).

The newly developed method can find potential applications for high-speed surface free energy mapping over large areas in super-hydrophobic heterogeneous materials, where a spatially informed measurement of adhesive properties is needed for the development of new materials with tailored wettability.

Methodology

Samples under investigation

The samples used as a reference consisted of a commercially sourced germanium (100) wafer (Neyco.fr) and mica natural crystals (Ruby Mica Co. LTD.). Mica is a silicate mineral in sheet form that can be easily cleaved to create atomically flat and defect-free surfaces, by using the scotch tape method like the one adopted to obtain graphene from graphite (cleavage method). The water contact angle of the mica surfaces was observed to be unstable for some minutes after cleavage [53].

Hence, all testing on mica was performed after a waiting time of at least 30 min after preparation.

Hydrophobic flat reference samples were obtained by gas phase deposition of fluorinated silane ($C_{10}H_4F_{17}Si$) over the flat germanium substrates (silanization process). Before deposition, an oxygen plasma treatment is performed, which creates Ge–OH groups on the surface. Ge–OH reacts with the silanes of perfluorodecyltrichlorosilane (FDTS) and forms a hydrophobic single layer on the surface.

Finally, the nano-patterned super-hydrophobic material [54] was obtained by e-beam lithography, using the process described in Fig. 9b. A metallic mask is deposited on the germanium substrate by sputtering and patterned with high-resolution lithography and etching steps. The patterns are then transferred onto the substrate using a SF6 based ICP/RIE plasma. The isotropic component of the plasma enables formation of nanostructures with conical shapes. The metallic mask is finally removed in an acid solution and the samples are subsequently cleaned.

The above-mentioned silanization process was also carried out on the nanopatterned sample to study the effects on wettability of the combination of the two methods.

Contact angle measurements

Wettability and surface energy were also measured by contact angle experiments, according to the procedures described in UNI EN 828, UNI 9752, ASTM D-5725–99 standards. To evaluate surface energy and its components (polar, non-polar), three different liquids can be used: distilled water and formamide (AnalaR NORMAPUR®) as polar liquids; methylene iodide (Merck Millipore) as non-polar liquid. To be able to calculate SFE, data on at least two liquids (one polar, one non-polar) are obtained. The values of the polar and dispersive components of the surface tensions of the liquids were found in literature from the works of van Oss et. Al. and Chaudhury [55–57]. Testing was performed in a controlled environment (temperature 20–22 °C, relative humidity 25–35%). Six drops (with a volume of 3 µl) were deposited for each liquid. After the acquisition and processing of the images, contact angles values from at least two liquids (one polar, one non-polar) are used to calculate the total surface energy and the two components (dispersion, polar) using the Owens–Wendt method [58]. Since CA measurements require a large area for depositing the droplets (at least 5×5 cm^2 in the present case), surface energy analysis have been limited to water contact angle measurements with 1.5 µl on the nanopatterned sample.

Nanoindentation measurements

Nanoindentation measurements were performed using a Nanoindenter iNano from KLA-Nanomechanics, equipped
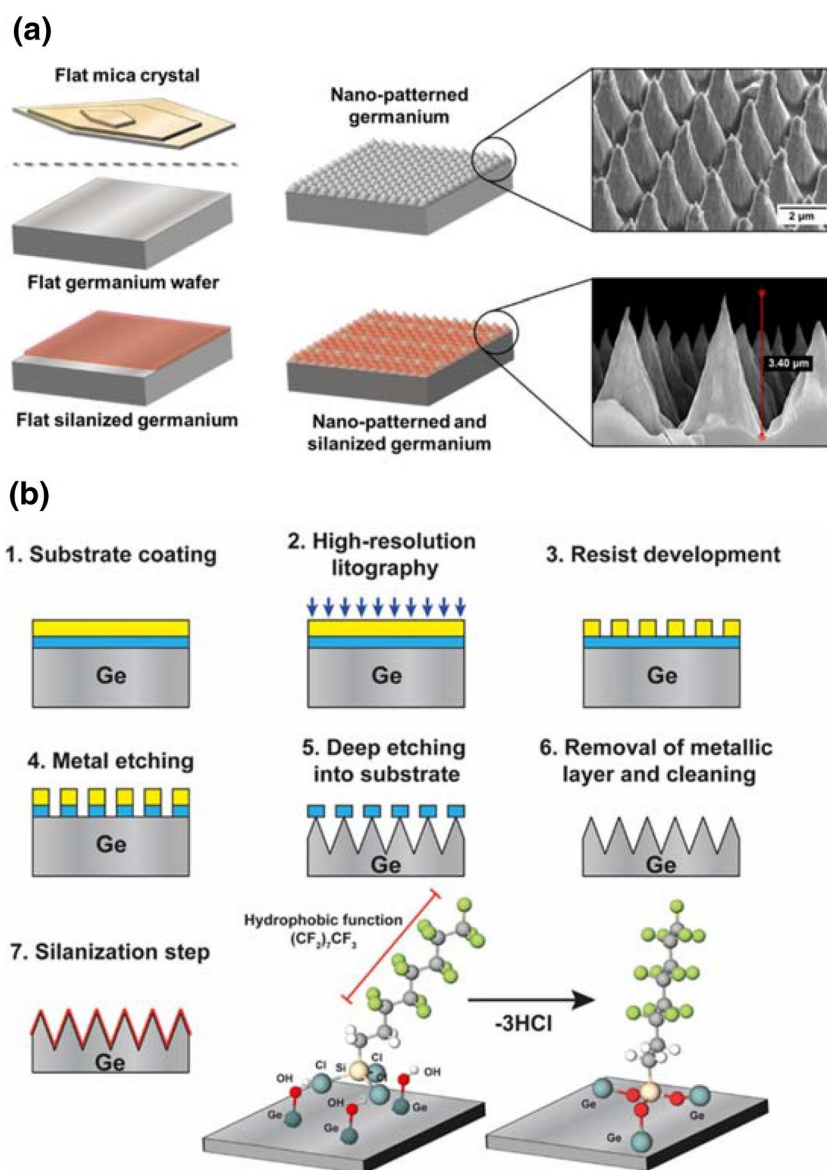
with a modified inForce50 actuator (spring stiffness 716 N/m).
To reduce the maximum load from 50 to 5 mN, a device limit-
ing the maximum current to the magnetic coil in the actuator
(called "force concentrator") was used. In this way, the force
resolution is further improved and the associated RMS value
of force, considering the dynamics of the instrument, is below
0.21 μN. In the case of surface energy measurements, tests were
performed by using two different sphero-conical tips, with a
radius of 52.5 μm and 15.8 μm, respectively. The experiments
are performed in pseudo-displacement control mode, with an
approaching speed of 2–5 nm/s. After the contact, the same
velocity is maintained until a fixed number of data points, cali-
brated to ensure that the displacement into surface is kept below
5 nm (which roughly corresponds to a maximum load of 5–10
μN for the flat reference samples), is acquired. In this way, a

purely elastic deformation of the samples surfaces is ensured.
For the mica sample tested with the 52.8 um tip, a long-range
sample-tip interaction can be noticed (see Fig. 5a) before the
real snap-in event. Presumably, this is due to induced artifacts
(e.g., detached layers remaining on the surface, electrostatic
long-range polar interactions) from the cleavage process used
to create a fresh surface for this material which are cancelled
during contact, and hence not considered in the pull-off based
surface energy calculations.

With regard to the selection of the indenter tip, it is worth
noting that, in principle, the Berkovich geometry could also be
used for SFE measurement. However, the pull-off forces would
be reduced significantly (in comparison with a large spherical
indenter) and a very sharp tip cannot be used on nano-patterned
materials, since the indenter would fall in between two adjacent

cones in most of the cases. Using a Berkovich tip on flat surfaces with a large penetration depth of the indenter into the surface, results in a large contact area and precise measurement of pull-off force. However, in such cases the effective indenter shape [45, 46] should be used for SFE calculation, as the "effective" tip radius. Such a solution may be a good alternative to spherical tips in case of SFE measurement on soft materials.

For the nanopatterned samples, the testing procedure was set to have a maximum load not higher than 5 μN. In addition to using an improved actuator, the entire nanoindentation system is installed inside a glovebox to carefully control the humidity (RH 8% ± 4%) and temperature (23.0 ± 0.2 °C) during testing (the glovebox system is shown in Figure I in the supplementary material), resulting in enhanced thermal and environmental stability. The spring stiffness calibration was performed under the same environmental conditions, before and after each series of tests. Tip cleaning was performed after each series of experiments, by using isopropyl alcohol in ultrasonic bath. In all cases, the presence of a clear pull-off force on the reference Germanium sample was an indicator of a properly cleaned tip. Therefore, a series of tests on the reference germanium was also performed before and after each new sample. After testing, the measured pull-off force was used to calculate the material's Surface Free Energy (SFE), by using both the JKR and DMT models. At least 20 valid measurements for each sample were used. The reference SFE of the diamond indenter was taken from the literature, equal to 43 mJ/m^2 [59].

Acknowledgments

Funding

Compliance with ethical standards

Conflict of interest The authors declare that they have no known competing financial interests or personal relationships that could have appeared to influence the work reported in this paper.

Supplementary information

The online version contains supplementary material available at https://doi.org/10.1557/s43578-021-00127-3.

Open access

References

1. R. Hensel, K. Moh, E. Arzt, Adv. Funct. Mater. **28**, 1800865 (2018)

2. T. Mouterde, G. Lehoucq, S. Xavier, A. Checco, C.T. Black, A. Rahman, T. Midavaine, C. Clanet, D. Quéré, Antifogging abilities of model nanotextures. Nat. Mater. **16**(6), 658 (2017)

3. V. Barreau, R. Hensel, N.K. Guimard, A. Ghatak, R.M. McMeeking, E. Arzt, Fibrillar elastomeric micropatterns create tunable adhesion even to rough surfaces. Adv. Funct. Mater. **26**(26), 4687 (2016)

4. Q. Cai, B. Xu, L. Ye, T. Tang, S. Huang, X. Du, X. Bian, J. Zhang, Z. Di, Q. Jin, J. Zhao, Stable functionalization of germanium surface and its application in biomolecules immobilization. Appl. Surf. Sci. **316**(1), 46 (2014)

5. A. Malshe, K. Rajurkar, A. Samant, H.N. Hansen, S. Bapat, W. Jiang, Bio-inspired functional surfaces for advanced applications. CIRP Ann. - Manuf. Technol. **62**(2), 607 (2013)

6. A.M. Kietzig, S.G. Hatzikiriakos, P. Englezos, Patterned superhydrophobic metallic surfaces. Langmuir **25**(8), 4821 (2009)

7. Y.P. Zhao, L.S. Wang, T.X. Yu, J. Adhes. Sci. Technol. **17**, 519 (2003)

8. L. Ponsonnet, K. Reybier, N. Jaffrezic, V. Comte, C. Lagneau, M. Lissac, C. Martelet, Relationship between surface properties (roughness, wettability) of titanium and titanium alloys and cell behaviour. Mater. Sci. Eng. C **23**(4), 551 (2003)

9. B. Banerjee, S.K. Roy, Physics of binding between cell-adhesion molecules (CAMs) in biosamples. Indian J. Phys. **77**(2), 187 (2003)

10. S.K. Tran, Adhesion issues in flip-chip on organic modules. IEEE Trans. Comp. Packag. Technol. **22**(4), 519 (1999)

11. Y. He, X. Zhang, R.D. Hooton, X. Zhang, Effects of interface roughness and interface adhesion on new-to-old concrete bonding. Constr. Build. Mater. **151**, 582 (2017)

12. N. Tan, Z.G. Xing, X.L. Wang, H.D. Wang, G. Jin, B.S. Xu, Effects of texturing patterns on the adhesion strength of atmosphere plasma sprayed coatings. J. Mater. Res. **32**(9), 1682 (2017)

13. K. Mozaffari, S. Yang, P. Sharma, in *Handb. Mater. Model.* (2020), pp. 1949–1974.

14. M. Ciavarella, J. Joe, A. Papangelo, J.R. Barber, J. R. Soc. Interface **16**, 20180738 (2019)

15. B. Derkus, Applying the miniaturization technologies for biosensor design. Biosens. Bioelectron. **79**, 901 (2016)

16. H. Pfaff, Synthesis and adhesion of biomimetic contact elements. *Structure* No. 191 (2007).

17. B. Bhushan, Y.C. Jung, K. Koch, Micro-, nano- And hierarchical structures for superhydrophobicity, self-cleaning and low adhesion. Philos. Trans. R. Soc. A **367**(1894), 1631 (2009)

18. S. Khandavalli, P. Rogers, J.P. Rothstein, Roll-to-roll fabrication of hierarchical superhydrophobic surfaces. Appl. Phys. Lett. **113**(4), 1 (2018)

19. A.M. Kietziga, M.N. Mirvakilia, S. Kamalb, P. Englezosa, S.G. Hatzikiriakosa, Nanopatterned metallic surfaces: their wettability and impact on ice friction. J. Adhes. Sci. Technol. **25**(12), 1293 (2011)

20. V. Belaud, S. Valette, G. Stremsdoerfer, M. Bigerelle, S. Benayoun, Wettability versus roughness: multi-scales approach. Tribol. Int. **82**(PB), 343 (2015)

21. Y.I. Rabinovich, J.J. Adler, A. Ata, R.K. Singh, B.M. Moudgil, Adhesion between nanoscale rough surfaces. I. Role of asperity geometry. J. Colloid Interface Sci. **232**(1), 10 (2000)

22. T. Huhtamäki, X. Tian, J.T. Korhonen, R.H.A. Ras, Surface-wetting characterization using contact-angle measurements. Nat. Protoc. **13**(7), 1521 (2018)

23. F.M. Etzler, Determination of the surface free energy of solids: a critical review. Rev. Adhes. Adhes. **1**(1), 3 (2013)

24. F.M. Borodich, B.A. Galanov, Non-direct estimations of adhesive and elastic properties of materials by depth-sensing indentation. Proc. R. Soc. A **464**(2098), 2759 (2008)

25. I.L. Jäger, Surface free energy—a possible source of error in nanohardness? Surf. Sci. **565**(2–3), 173 (2004)

26. F. Awaja, M. Gilbert, G. Kelly, B. Fox, P.J. Pigram, Adhesion of polymers. Prog. Polym. Sci. **34**(9), 948 (2009)

27. W.W. Gerberich, M.J. Cordill, Physics of adhesion. Rep. Prog. Phys. **69**(7), 2157 (2006)

28. U. Landman, W.D. Luedtke, N.A. Burnham, R.J. Colton, Atomistic mechanisms and dynamics of adhesion, nanoindentation, and fracture. Science **248**(4954), 454 (1990)

29. R.S. Bradley, LXXIX. The cohesive force between solid surfaces and the surface energy of solids. London, Edinburgh, Dublin Philos. Mag. J. Sci. **13**(86), 853 (1932).

30. B.V. Derjaguin, V.M. Muller, Y.P. Toporov, Effect of contact deformation on the adhesion of elastic solids. J. Colloid Interface Sci. **53**(2), 314 (1975)

31. B.V. Derjaguin, V.M. Muller, Y.P. Toporov, Effect of contact deformations on the adhesion of particles. J. Colloid Interface Sci. **53**, 314 (1975)

32. K.L. Johnson, K. Kendall, A.D. Roberts, Surface energy and the contact of elastic solids. Proc. R. Soc. Lond. A **324**(1558), 301 (1971)

33. J. Song, G.J. Vancso, Effects of flame treatment on the interfacial energy of polyethylene assessed by contact mechanics. Langmuir **24**(9), 4845 (2008)

34. D. Tabor, Surface forces and surface interactions. J. Colloid Interface Sci. **58**(1), 2 (1977)

35. V.M. Muller, V.S. Yushchenko, B.V. Derjaguin, On the influence of molecular forces on the deformation of an elastic sphere and its sticking to a rigid plane. J. Colloid Interface Sci. **77**(1), 91 (1980)

36. K.L. Johnson, J.A. Greenwood, An adhesion map for the contact of elastic spheres. J. Colloid Interface Sci. **192**(2), 326 (1997)

37. N.K. Myshkin, M.I. Petrokovets, A.V. Kovalev, Tribology of polymers: adhesion, friction, wear, and mass-transfer. Tribol. Int. **38**, 910 (2005)

38. D. Maugis, Adhesion of spheres: the JKR-DMT transition using a dugdale model. J. Colloid Interface Sci. **150**(1), 243 (1992)

39. H.J. Butt, B. Cappella, M. Kappl, Surf. Sci. Rep. **59**, 1 (2005)

40. Y. Zhang, Y. Oh, D. Stauffer, A.A. Polycarpou, A microelectro-mechanical systems (MEMS) force-displacement transducer for sub-5 nm nanoindentation and adhesion measurements. Rev. Sci. Instrum. **89**(4), 045109 (2018)

41. E. Yu, S.C. Kim, H.J. Lee, K.H. Oh, M.W. Moon, Extreme wettability of nanostructured glass fabricated by non-lithographic, anisotropic etching. Sci. Rep. **5**, 2 (2015)

42. P.S. Phani, W.C. Oliver, Ultra high strain rate nanoindentation testing. Materials (Basel) **10**(6), 663 (2017)

43. X. Xu, G. Vereecke, C. Chen, G. Pourtois, S. Armini, N. Verellen, W.K. Tsai, D.W. Kim, E. Lee, C.Y. Lin, P. Van Dorpe, H. Struyf, F. Holsteyns, V. Moshchalkov, J. Indekeu, S. De Gendt, Capturing wetting states in nanopatterned silicon. ACS Nano **8**(1), 885 (2014)

44. K. Xiao, Y.P. Zhao, G. Ouyang, X.L. Li, An analytical model of nanopatterned superhydrophobic surfaces. J. Coatings Technol. Res. **14**(6), 1297 (2017)

45. A. Bolshakov, W.C. Oliver, G.M. Pharr, in *Mater. Res. Soc. Symp. - Proc.* (1995).

46. G. M. Pharr and A. Bolshakov: Understanding nanoindentation unloading curves. *J. Mater. Res.* (2002).

47. T. Shadloo, S. Firoozi, P. Marashi, A. ZolfaghariHesari, M. Rezaee, S. Jalilzadeh, Determination of the adhesion properties of mica via atomic force spectroscopy. Int. J. Mod. Phys. Conf. Ser. **05**, 33 (2012)

48. A. Relini, S. Sottini, S. Zuccotti, M. Bolognesi, A. Gliozzi, R. Rolandi, Measurement of the surface free energy of streptavidin crystals by atomic force microscopy. Langmuir **19**(7), 2908 (2003)

49. W.C. Oliver, G.M. Pharr, An improved technique for determining hardness and elastic modulus using load and displacement sensing indentation experiments. J. Mater. Res. **7**(6), 1564 (1992)

50. J.N. Israelachvili, P.M. McGuiggan, Adhesion and short-range forces between surfaces. Part i: New apparatus for surface force measurements. J. Mater. Res. **5**(10), 2223 (1990)

51. P.M. McGuiggan, J.N. Israelachvili, Adhesion and short-range forces between surfaces. Part II: effects of surface lattice mismatch. J. Mater. Res. **5**(10), 2232 (1990)

52. B. Vignesh, W.C. Oliver, G.S. Kumar, P.S. Phani, Critical assessment of high speed nanoindentation mapping technique and data deconvolution on thermal barrier coatings. Mater. Des. **181**, 108084 (2019)

53. H.K. Christenson, Adhesion and surface energy of mica in air and water. J. Phys. Chem. **97**(46), 12034 (1993)

54. E. Martines, K. Seunarine, H. Morgan, N. Gadegaard, C.D.W. Wilkinson, M.O. Riehle, Superhydrophobicity and superhydrophilicity of regular nanopatterns. Nano Lett. **5**(10), 2097 (2005)

55. C.J. van Oss, *Interfacial Forces in Aqueous Media*, 2nd ed. (2006).

56. M.K. Chaudhury, *Short-Range and Long-Range Forces in Colloidal and Macroscopic Systems* (State University of New York, 1984).

57. C.J.V. Oss, R.J. Good, H.J. Busscher, Estimation of the polar surface tension parameters of glycerol and formamide, for use in contact angle measurements on polar solids. J. Dispers. Sci. Technol. **11**(1), 75 (1990)

58. D.K. Owens, R.C. Wendt, Estimation of the surface free energy of polymers. J. Appl. Polym. Sci. **13**(8), 1741 (1969)

59. L. Mazzola, M. Sebastiani, E.E. Bemporad, F.F. Carassiti, An innovative non-contact method to determine surface free energy on micro-areas. J. Adhes. Sci. Technol. **26**(1–3), 131 (2012)